JGR Earth Surface

RESEARCH ARTICLE
10.1029/2021JF006570

The Relative Impacts of Initialization and Climate Forcing in Coupled Ice Sheet-Ocean Modeling: Application to Pope, Smith, and Kohler Glaciers

D. N. Goldberg[1] and **P. R. Holland**[2]

[1]School of Geosciences, University of Edinburgh, Edinburgh, UK, [2]British Antarctic Survey, Cambridge, UK

Key Points:

- Different initialization strategies, sliding laws, and climate forcings are applied to a coupled ice sheet-ocean model
- Grounded ice loss rates are determined by model initialization in the first 1–2 decades, but controlled by forcing over longer time scales
- Despite the influence of forcing, overall grounding line retreat is affected as strongly by initialization as by forcing for 50-year simulations

Supporting Information:

Supporting Information may be found in the online version of this article.

Correspondence to:

D. N. Goldberg,
dan.goldberg@ed.ac.uk

Citation:

Goldberg, D. N., & Holland, P. R. (2022). The relative impacts of initialization and climate forcing in coupled ice sheet-ocean modeling: Application to Pope, Smith, and Kohler glaciers. *Journal of Geophysical Research: Earth Surface*, *127*, e2021JF006570. https://doi.org/10.1029/2021JF006570

Received 16 DEC 2021
Accepted 10 MAY 2022

Abstract Coupled ice sheet-ocean models are beginning to be used to study the response of ice sheets to ocean warming. Initializing an ice-ocean model is challenging and can introduce nonphysical transients, and the extent to which such transients can affect model projections is unclear. We use a synchronously-coupled ice-ocean model to investigate evolution of Pope, Smith and Kohler Glaciers, West Antarctica, over the next half-century. Two methods of initialization are used: In one, the ice-sheet model is constrained with observed velocities in its initial state; in another, the model is constrained with both velocities and grounded thinning rates over a 4-year period. Each method is applied to two basal sliding laws. For each resulting initialization, two climate scenarios are considered: one where ocean conditions during the initialization period persist indefinitely, and one where the ocean is in a permanent "warm" state. At first, model runs initialized with thinning data exhibit volume loss rates much closer to observed values than those initialized with velocity only, but after 1–2 decades, the forcing primarily determines rates of volume loss and grounding line retreat. Such behavior is seen for both basal sliding laws, although volume loss rates differ quantitatively. Under the "warm" scenario, a grounding line retreat of ~30 km is simulated for Smith and Kohler, although variation in total retreat due to initialization is nearly as large as that due to forcing. Furthermore it is questionable whether retreat will continue due to narrowing of submarine troughs and limiting of heat transport by bathymetric obstacles.

Plain Language Summary In a number of locations along the Antarctic coastline, particularly in West Antarctica, warm waters which originate in the midlatitudes exist on the continental shelf, protected from cold air and freezing conditions at the surface. These warm waters are able to circulate underneath ice shelves—The vast floating extensions of fast-flowing outlet glaciers—Leading to high levels of melt and thinning. The thinning, in turn, drives speedup and thinning of the glaciers, contributing to rising sea levels. To study this process, interactive models of ice dynamics and ocean circulation are used. As in other areas of Earth System modeling, such as weather prediction, the way in which these models are initialized impacts model predictions, and due to the complexity of interactions between ice and ocean, these impacts are poorly understood. Here, we use a novel model of ice-ocean interaction and consider different ways of initializing the model using remotely-observed data, applied to a very fast-thinning system of West Antarctic glaciers. We find that 10–20 years predictions of ice-ocean evolution depend strongly on initialization, but longer-term predictions depend more on evolving climate.

1. Introduction

Roughly half of the mass output from the Antarctic Ice Sheet is due to melting of ice shelves (Depoorter et al., 2013). Much of this melt is concentrated in sectors of the Antarctic coastline where Circumpolar Deep Water (CDW) is able to circulate on the continental shelf due to factors such as wind forcing, lower sea ice growth, and deep oceanic troughs, for instance the Amundsen Sea in West Antarctica (Dutrieux et al., 2014; Jenkins et al., 2018; Petty et al., 2013). Under ice shelves in the Amundsen Sea, melt rates can reach tens or even hundreds of meters per year of ice removal (Dutrieux et al., 2013; Gourmelen et al., 2017; Khazendar et al., 2016; Milillo et al., 2019). The ice streams that flow into these fast-thinning ice shelves have accelerated in response to the associated loss of ice-shelf buttressing (Mouginot et al., 2014; Shepherd et al., 2004), resulting in increased grounded mass loss and grounding-line retreat (B. Smith et al., 2020; Rignot et al., 2014; Scheuchl et al., 2016; Shepherd et al., 2018). Grounding line retreat is of particular concern when considering the contribution of these ice streams to the sea level due to their inland-deepening beds, as retreat of the grounding line can expose newly

floating ice to deeper, warmer waters, which can drive further melt (Jacobs et al., 2011). Additionally, grounding line retreat into deeper-bedded regions can potentially lead to faster flow and retreat (e.g., Schoof, 2007)—Although factors such as buttressing, bed curvature, self-gravitation, and temperature-elevation feedback can provide negative feedback on such acceleration (Gomez et al., 2010; Haseloff & Sergienko, 2018; Pegler, 2018; Schoof et al., 2017; Sergienko, 2022; Sergienko & Wingham, 2022).

A number of ice-sheet modeling studies have examined the response of fast-flowing Amundsen glaciers to ocean forcing (e.g., Dos Santos et al., 2021; Favier et al., 2014; Joughin et al., 2014; Lilien et al., 2019), the majority of which have used a depth-dependent parameterization for melting. Such parameterizations largely neglect the influence of the ocean circulation in ice-shelf cavities, leading to important deficiencies in both the spatial distribution of melting, and the ice-shelf response to changes in ocean forcing. To properly represent the complexity of ocean forcing of ice shelf melt, a coupled ice-ocean model is needed.

There have been an increasing number of coupled ice sheet-ocean studies in recent years (De Rydt & Gudmundsson, 2016; Favier et al., 2019; Goldberg et al., 2012a; Grosfeld & Sandhager, 2004; J. R. Jordan et al., 2017; Naughten et al., 2021; Pelle et al., 2021; R. S. Smith et al., 2021; Seroussi et al., 2017; Snow et al., 2017; Timmermann & Goeller, 2017), and coupled ice-ocean development has advanced to the point where model intercomparisons are now being carried out (Asay-Davis et al., 2016). A large number of these studies have been idealized, initialized in a quiescent state; in reality, a number of Antarctic ice streams are in a highly dynamic state, as a result of ocean-forced melting. In the InitMIP-Antarctica intercomparison (Seroussi et al., 2019), a number of different ice-sheet models were initialized through different methods, with strongly diverging responses to ice-shelf melt for century-scale simulations. In a coupled ice-ocean model, there is an additional complexity relating to the fact that under-ice circulation (and thus melt) depends strongly on ice-shelf geometry. Thus uncertainty in the initial dynamic state of the ice sheet-ice shelf system can potentially be amplified through melt uncertainty, which feeds back on ice-shelf geometry. A commonly-used ice-sheet initialization strategy is to minimize the misfit of ice-model velocities with those observed via satellite imagery (Naughten et al., 2021; Seroussi et al., 2017), although some studies consider a trade-off between velocities and fit to observed thinning trends of grounded ice (Arthern et al., 2015; Goldberg et al., 2019), effectively controlling the ice-sheet model over a finite time period rather than an instant.

It remains unclear the degree to which the initialization strategy (as well as structural aspects of ice-sheet models) influences multidecadal-scale evolution in coupled ice-ocean models, relative to climatic forcing. This is an important question, as it bears on whether accurate climate predictions in global and regional circulation models can lead to accurate predictions in coupled ice-ocean models, or whether internal variability of the ice sheet—That is detailed interactions with the bed and response to ice-shelf thinning—Must be captured. An aim of this study is to understand whether forcing or initial state more strongly controls the multidecadal evolution of ice streams.

In the following, we describe our methodologies for initialization and multidecadal simulation of coupled ice-ocean dynamics of a fast-thinning Amundsen region, the Pope, Smith and Kohler (PSK) glaciers. Previously Goldberg et al. (2015) showed that continued grounding-line retreat and thinning is likely even if loss of buttressing due to ocean melt were to cease. The study of Lilien et al. (2019) suggested that, at least in past decades, the glaciers were not inherently unstable despite bed morphology, and sustained ocean-driven melt was required to drive the amount of retreat observed. The study further showed that, under these same conditions, retreat would likely continue throughout the 21st century. Neither of these studies considered the effects of ocean circulation in controlling present and future melt rates: Goldberg et al. (2015) disregarded ice-shelf forcing entirely, while Lilien et al. (2019) used a depth-dependent melt parameterization as described above.

We test a range of coupled model initialization strategies, including fitting to velocities and to thinning trends, both instantaneously and over a finite period. We consider two different scenarios of far-field ocean forcing, a "warm" and "cool" scenario. We additionally examine the effects of the basal sliding law. We present and discuss our results in the context of the relative importance of forcing and initialization, and the response of the PSK glaciers to climate forcing and their potential evolution during the 21st century.

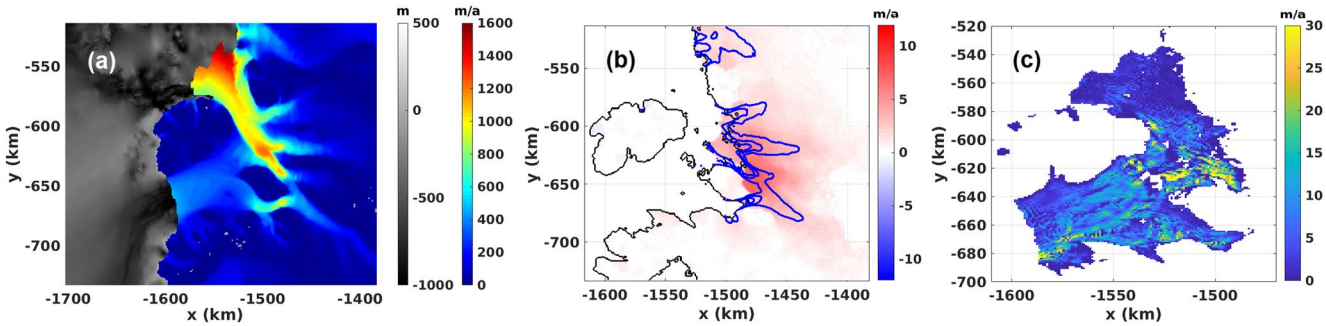

Figure 1. (a) MEaSUREs v2 ice surface speed within the model domain, overlain on ocean bathymetry (grayscale). (b) 2011–2015 thinning rates from CryoSat (shading). Blue lines are contours of surface speed over grounded ice (spacing 300 m/a) and the black contour represents the BedMachine grounding line. (c) Mean 2011–2015 melt rate from Massachusetts Institute of Technology's general circulation model ocean model with unchanging ice geometry Note axis scales differ between the figures. Geographic location of study area shown as inset in (a).

2. Region of Study

The PSK glaciers are three such fast-thinning, fast-retreating Amundsen glaciers (See Figure 1 for geographic reference). While the region of the Antarctic Ice Sheet drained by these glaciers is small relative to that of nearby Pine Island and Thwaites glaciers, throughout the satellite observing record, they have exhibited some of the highest retreat rates in Antarctica, with their grounding lines receding over 30 km in recent decades (Scheuchl et al., 2016). A large proportion of the PSK catchment underwent strong thinning rates between 2011 and 2015 (Figure 1), with thinning concentrated toward the grounding lines of the connecting Crosson and Dotson Ice Shelves. During roughly the same period, the grounded mass balance of PSK was similar to that of Thwaites Glacier, despite covering an area 1/5 the size (Table 1 of McMillan et al., 2014). At the same time, Dotson and Crosson Ice Shelves, the ice shelves into which the PSK glaciers flow, have experienced strong melt rates driven by influx of CDW (Goldberg et al., 2019; Gourmelen et al., 2017; Jenkins et al., 2018). The coincident strong melting and thinning suggests an ocean driver of ice loss, and the continued retreat of the grounding line into deeper-bedded areas raises concern regarding the potential for rapid collapse of the glaciers. Indeed, extrapolation of current ice-shelf thinning suggests that Dotson will melt through before the end of the century (Gourmelen et al., 2017), which could potentially lead to a strong loss of buttressing and accelerated speedup (Goldberg et al., 2012b; Reese et al., 2018). The PSK catchment can potentially contribute 6 cm to the global sea level (Morlighem et al., 2020), almost 20% of that of the entire inventory of Earth's mountain glaciers (Farinotti et al., 2019)—And a complete collapse would likely lead to accelerated loss from adjacent ice streams, including Thwaites Glacier. As such, it is important to understand how the PSK region may respond to climate drivers in the future.

3. Methods

3.1. Coupled Ice-Ocean Modeling

3.1.1. Ocean Model

We use the Massachusetts Institute of Technology's general circulation model (MITgcm; Marshall et al., 1997) to model ocean circulation and melt under Dotson and Crosson ice shelves. We use a stereographic polar projected grid with 1 km resolution, which covers the ice shelves, ice streams, and a small portion of open ocean in front of the ice shelves (*cf.* Figure 1a). Sub-ice shelf melt rates are calculated via the sublayer parameterization of D. M. Holland and Jenkins (1999), using the implementation of Losch (2008). A velocity-dependent melt rate calculation is used (Dansereau et al., 2014), in which the friction velocity u_* is given by

$$u_*^2 = C_D|U|^2 \tag{1}$$

where $|U|$ is the norm of the near-ice ocean velocity. We set $C_D = 0.006$, which yielded a good fit to satellite- and ocean-observed melt rates for the period 2011–2015 (Goldberg et al., 2019). The model setup is similar to that of Goldberg et al. (2019), with the exception that vertical resolution is 25 m instead of 20 m; and BedMachine Antarctica v2 (Morlighem et al., 2020) is used for ice thickness and bathymetry rather than Bedmap2 (Fretwell

et al., 2013) and Millan et al. (2017), respectively. Additionally, there are minor changes in the treatment of viscosity related to the ice-ocean coupling strategy, as described below.

As in Goldberg et al. (2019), far-field ocean conditions (temperature, salinity and velocity) are imposed at the ocean-facing boundaries, taken from monthly outputs of the regional simulation of Kimura et al. (2017). The simulation of Kimura, in turn, was forced by ERA-Interim reanalysis, and can be considered an adequate product for this part of the Amundsen region. In our model, sea-ice and atmospheric surface forcing is not considered because the impact of such forcing over the relatively small area of open ocean on waters at depth is expected to be minor. However, the neglect of atmospheric cooling may mean that ocean temperatures at depth could be slightly overestimated.

3.1.2. Ice-Sheet Model

The ice sheet-ice shelf model is STREAMICE, a physical "package" of MITgcm (Goldberg & Heimbach, 2013). STREAMICE implements the stress balance of Goldberg (2011), which is a depth-integrated balance appropriate for both slow deformational and fast-sliding and floating regimes (see also Arthern et al. (2015) and Lipscomb et al. (2019)). Two sliding laws are considered in coupled initializations and simulations: a Weertman sliding law, which takes the form

$$\tau_b = \beta^2 \left(u_b^2 + u_0^2\right)^{(1-m)/(2m)} u_b, \tag{2}$$

and a "Coulomb-regularized" or "Coulomb-limited" Weertman sliding law (Cornford et al., 2020; Lilien et al., 2019):

$$\tau_b = \frac{\alpha^2 \beta^2 u_b^{1/m} N_{eff}}{\left[\beta^{2m} u_b + (\alpha^2 N_{eff})^m\right]^{1/m}} \tag{3}$$

where N_{eff} is effective pressure, parameterized by ice overburden minus hydrostatic ocean pressure. Effectively, basal stress behaves according to a Coulomb sliding law near the grounding line, but transitions to a Weertman-type law further inland. As in Cornford et al. (2020), m is 3 and α is 0.5. A value of $u_0 = 10^{-8}$ m/a is used to regularize the Weertman law. Each initialization and coupled experiment described below is carried out twice, once with each sliding law. β^2, the sliding parameter, is spatially varying, as is $\bar{B}$, the ice stiffness coefficient in the nonlinear viscosity formulation (Equation 16 of Goldberg, 2011):

$$\nu = \frac{\bar{B}}{2}\left[\left(\frac{\partial \bar{u}}{\partial x}\right)^2 + \left(\frac{\partial \bar{v}}{\partial y}\right)^2 + \left(\frac{\partial \bar{u}}{\partial x}\right)\left(\frac{\partial \bar{v}}{\partial y}\right) + \frac{1}{4}\left(\frac{\partial \bar{v}}{\partial x} + \frac{\partial \bar{u}}{\partial y}\right)^2 + \frac{1}{4}\left(\frac{\partial u}{\partial z}\right)^2 + \frac{1}{4}\left(\frac{\partial v}{\partial z}\right)^2 + \epsilon_0^2\right]^{\frac{1-n}{2n}}, \tag{4}$$

where $\bar{u}$ is depth-averaged x-velocity, and similar for other terms, and $n = 3$. Background strain rate ϵ_0 is 10^{-8} a^{-1} in all experiments. Both β^2 and $\bar{B}$ are set as described in Section 3.2. For time-dependent model runs, the model is forced with surface mass balance derived from RACMO 2.1 output (Lenaerts et al., 2012).

3.1.3. Model Coupling

STREAMICE is coupled to the MITgcm ocean model with the scheme described in Goldberg et al. (2018). The coupling between ice and ocean is *synchronous*: the geometry of the ice sheet and shelf coevolve with the ocean on a common grid and on the ocean time step (J. R. Jordan et al., 2017). This is in contrast to an asynchronous scheme, where the ice geometry remains constant over a much longer time period (e.g., 1 month or 1 year), whereupon it is updated and the ocean model is reinitialized with a new geometry, with the properties of new ocean cells filled via an extrapolation scheme (De Rydt et al., 2014; Goldberg et al., 2012a; Naughten et al., 2021).

As described in Goldberg et al. (2018), a thin ocean layer exists everywhere under the ice sheet. This regularization is necessary due to the implicit free-surface solver in the MITgcm ocean model: An ocean column must have nonzero thickness in order to expand when ice thins and goes afloat. In a grounded ice-sheet cell adjacent to the ice shelf, when the ice thins to floatation thickness, water flows in from the ice-shelf cavity and the column expands. In this manner mass, temperature and salinity are conserved within the domain. In this study, a minimum water column thickness (MWCT) of 2 m is used, and temperature and salinity in the sub-ice sheet layer are initialized similarly to the rest of the ocean model (see Section 3.2). Additionally, ice-shelf melt (and associated

thermodynamic forcing of ocean surface) is prevented when the ocean column is less than 5 m. A sensitivity assessment of these parameters is outside the scope of the present study; but in Goldberg et al. (2018) a comprehensive parameter analysis showed that a number of parameters relating to the coupling scheme—Including MWCT, initial layer temperature, and minimum thickness for melt to occur—Had negligible effect on coupled model evolution.

As a result of the formulation of J. R. Jordan et al. (2017), ocean melt is not applied in locations where ice-shelf draft is less than one grid cell thickness (25 m). Although not anticipated, such instances do occur in some of our simulations. Although this constraint prevents such areas from thinning further, they are assumed to carry negligible stress and considered to have "melted through" (see Section 5.2).

In initial experiments based on the design from a recent intercomparison (Asay-Davis et al., 2016), it was found that a strong, Coriolis-forced, melt-driven boundary current could exhibit instability, and the resulting fluctuations could cause the subglacial layer in grounded cells adjacent to the ice-shelf margin to collapse, crashing the simulation. Two adjustments were made to counter this effect: (a) A modified Leith viscosity (Fox-Kemper & Menemenlis, 2008) was used to lessen such instabilities, and (b) the vertical viscosity used in the formulation of implicit bottom drag (Goldberg et al., 2018) was increased by a constant factor for cells in the subglacial layer to add an additional damping of the flow. We use the same adjustments here, with Leith parameters viscC2Leith and viscC2LeithD both set to 1.0 with a minimum eddy viscosity of 30 m^2/s and a vertical viscosity factor of 10.

3.2. Coupled Initialization

3.2.1. Velocity-Based Initialization

To evolve, the ice-sheet model requires that the frictional and ice stiffness fields β^2 and $\bar{B}$ be initialized. These properties arise from complex and heterogeneous patterns of ice temperature, shear-driven crevassing, bed roughness and subglacial water pressures, and using uniform values would lead to a nonphysical state of the ice sheet. A common approach is to solve an *inverse* problem where misfit with observed velocities is found with respect to β^2 and $\bar{B}$, that is, the *control* parameters. The procedure is described in detail in the supplement of Goldberg et al. (2019) but main details are given here. A cost function J is defined as follows:

$$J = J\left\{\bar{B}, \beta\right\} = J_{vel} + \gamma_s^{\beta} J_{\beta} + \gamma_s^{B} J_B + \gamma_p^{B} J_p, \tag{5}$$

where the individual terms are defined as.

$$J_{vel} = \sum_i \frac{|\boldsymbol{u}_{s,i} - \boldsymbol{u}^*_{s,i}|^2}{2N\sigma^2_{u,i}} \tag{6}$$

$$J_{\beta} = \sum_i \frac{(\Delta_x \beta_i)^2 + (\Delta_y \beta_i)^2}{N} \tag{7}$$

$$J_B = \sum_i \frac{\left(\Delta_x \bar{B}_i\right)^2 + \left(\Delta_y \bar{B}_i\right)^2}{N} \tag{8}$$

$$J_p = \sum_{\text{grounded cells } i} \frac{\left(\bar{B}_i - \bar{B}_{i,0}\right)^2}{N}. \tag{9}$$

Here $\boldsymbol{u}_{s,i}$ and $\boldsymbol{u}^*_{s,i}$ are modeled and observed surface velocity vectors in cell i, respectively, $\sigma_{u,i}$ is observational uncertainty, β_i and $\bar{B}_i$ are the frictional and ice stiffness parameters in cell i, and N is the number of ice-covered cells in the domain. $\Delta_x(\chi_i)$ is the difference operator $\frac{1}{\Delta x}\left(\chi_i - \chi_{i_{left}}\right)$ for a cell-centered field χ where i_{left} indicates the left-lying cell to i, and $\Delta_y(\cdot)$ is defined similarly. γ_s^B, γ_s^{β}, and γ_p^B are parameters indicating the degree of imposed properties: regularity or, in the case of grounded ice stiffness, closeness to a prior $\bar{B}_0$. In the present study $\bar{B}_0$ is derived from the steady temperature solution calculated in Van Liefferinge and Pattyn (2013). "Grounded cells" are those cells where thickness H is above the floatation thickness $H_f = -(\rho_w/\rho_i)R$, where R is bathymetry. γ_s^B and γ_s^{β} are chosen based on an "L-surface" analysis (Fürst et al., 2015; Goldberg et al., 2019). For observed velocities the MEaSUREs (Rignot et al., 2011) Version 2 product is interpolated to the model domain

(Figure 1a). The misfit is then incrementally decreased using the large-scale optimization software M1QN3 (Gilbert & Lemaréchal, 1989), facilitated by finding the gradient of J at each iteration through an adjoint method (Goldberg & Heimbach, 2013). The initial guess for the parameters is a uniform value for β, and $\bar{B}$ equal to $\bar{B}_0$ over grounded ice and a uniform value for floating ice.

Meanwhile, the ocean model is spun up over the period 2009–2011 with fixed ice-shelf geometry, initialized with a spatially uniform salinity and temperature profile derived from 2009 output from Kimura et al. (2017). In Goldberg et al. (2019), 2 years was determined to be adequate spin-up time for this domain. Time-stepping of the coupled model then begins in 2011, using the optimized β^2 and $\bar{B}$ fields from above (with forcing as described in Section 3.3). This coupled initialization strategy, which we refer to as a "snapshot" approach, has been used by other coupling studies (Naughten et al., 2021; Seroussi et al., 2017).

3.2.2. Thinning-Based Initialization

In the "snapshot" approach described above, the inherent trends in thinning and volume loss of grounded ice are unconstrained. This introduces unphysical transients that might take decades to dissipate, which is not ideal for short-term prediction and validation. Hence, a second initialization strategy considered in this study involves controlling misfit between modeled and observed thinning over a finite reference period of time. The approach is again similar to that of Goldberg et al. (2019), but we give the main details. The cost function J defined above is augmented by an additional term:

$$J = J\{B, \beta\} = J_{vel} + \gamma_s^{\beta} J_{\beta} + \gamma_s^{B} J_B + \gamma_p^{B} J_p + \gamma_{tr} J_{trend}, \tag{10}$$

where

$$J_{trend} = \sum_{t=1}^{T_{tr}} \sum_i \frac{\left(\frac{1}{t}\left(H_i^t - H_i^0\right) - \left(\frac{dh}{dt}\right)^*\right)^2}{N}, \tag{11}$$

where H_i^t is model thickness in cell i at the end of year t of the simulation, and H_i^0 is initial thickness in cell i. $\left(\frac{dh}{dt}\right)^*$ is an *observed* thinning trend (discussed below), which does not vary in time, and γ_{tr} is a tuning parameter, which sets the relative importance of J_{trend}. The inner summation in Equation 11 is only over cells where ice is grounded, and where $\left(\frac{dh}{dt}\right)^*$ shows thinning of 1 m/a or greater. The latter constraint avoids constraining regions that are not dynamically coupled with the PSK glaciers, such as Bear and Martin Peninsulas. In addition, the velocities $\boldsymbol{u}_{s,i}$ in J_{vel} are *time-averaged* velocities, in order to avoid constraining velocities at only one point in time. The specific form of J_{trend}, whose terms involve mean thinning in the first, second and third year as well as the full reference period, is to avoid nonphysical behavior in the early years of the simulation. The run which generates H_i^t and $\boldsymbol{u}_{s,i}$ is forced by the time-mean of modeled ice-shelf melt from an ocean-only simulation over the reference period with fixed ice geometry, and RACMO-derived surface mass balance.

In our initialization, $\left(\frac{dh}{dt}\right)^*$ is from CryoSat-2 observations over the PSK region (Gourmelen et al. (2018); Figure 1b). 2011–2015 is chosen as the reference period; although there is a longer history of CryoSat-2 altimetry available, the Kimura et al. (2017) output does not extend past 2015. Moreover, the adjoint model for the transient initialization scales roughly with the number of time steps (Goldberg et al., 2016); thus, even longer reference periods would require even greater expense. It should be noted that the region over which $\left(\frac{dh}{dt}\right)^*$ implies thinning larger than 1 m/a is smaller than the entire PSK catchment. The region aligns well with the region of Ice Dynamical Imbalance from McMillan et al. (2014) and has a similar mean mass balance of -29.7 km^3/a (equivalently, -27.2 Gt/a with an ice density of 917 kg m^{-3}, or a mean thinning rate of 2.53 m/a). For the remainder of the paper the region of grounded ice and observed thinning over 1 m/a is referred to as the *IDI* region.

The rationale for the above design is as follows. If the ice model is optimized to fit with observed thinning trends in the absence of melt forcing, these trends will not necessarily be reproduced in the coupled model–especially if ice-shelf melt plays a strong role in grounded ice loss. On the other hand, if melt does not deviate strongly in the coupled model from that used in the initialization procedure, then the coupled model will exhibit strong fit with observed thinning. We refer to this initialization approach as "transient", as it uses a time-dependent ice-sheet model, although it does not use temporally resolved ice-sheet velocities. More importantly it *does not constrain*

in any way the melt rates or circulation of the ocean model. Rather, the comparison of modeled 2011–2015 melt against satellite data in Goldberg et al. (2019) is taken to indicate reasonable agreement between model and observations. Further, we note that previous ice sheet-climate initializations have considered bed topography as a control parameter (Perego et al., 2014). We do not do so here, but future strategies could consider doing so, with careful consideration of uncertainties.

In thinning-constrained initializations, the β and $\bar{B}$ resulting from corresponding "snapshot" initializations are used as initial guesses. The parameter γ_{tr} is chosen such that a significant reduction in J_{trend} is obtained without a strong increase in J_{vel} relative to the snapshot initialization.

A transiently-initialized coupled run then begins in 2011. The transiently- and snapshot-initialized coupled runs differ only in the β^2 and $\bar{B}$ fields of the ice-sheet model.

3.3. Climate Forcing

Since regional ocean model output after 2015 is not available for forcing, accurate future projections cannot be made within the context of this study. Instead, forcings are devised, which consider two possible scenarios regarding ocean temperatures in the western Amundsen Sea.

The strongest climatic impacts on ocean conditions under Amundsen ice shelves have come from interannual variability in wind forcing (Jenkins et al., 2016; Steig et al., 2012). Accordingly, 2011–2015, on average, was a relatively low-melting period for Dotson ice shelf compared to previous few years (Jenkins et al., 2018). The analysis of P. R. Holland et al. (2019) suggests that superimposed on this variability is a long-term trend in the intensifying of westerly wind stress at the Amundsen continental shelf break, a trend which is expected to continue under likely warming scenarios. Thus periods of warmer waters and shallower thermoclines on the continental shelf may occur more frequently in coming decades. In the first of our two scenarios, the 2011–2015 forcing is repeated on 4-year cycles. In the second, we force with a repeated annual cycle corresponding to the 2007 model output from Kimura et al. (2017), our choice based on the (post spin-up) year in which melt rates were highest in that model. We refer to these forcing scenarios as "Historical" and "Warm", respectively. In the "Warm" scenario, 2007-based forcing is not applied until 2015, so all coupled runs are forced identically over the first four years (*cf* Section 3.2.2). All experiments are run for 54 years each (2011–2015 plus 50 years with either repeated, or 2007-derived, forcing).

To summarize, there are four initializations: One for each sliding law and type of initialization. For each initialization, there are then two coupled simulations (i.e. Eight coupled experiments overall). All coupled experiments begin in 2011, with identical ice thickness and spun-up ocean conditions. The ocean-only simulation that produces the time-mean melt rate for the transient simulations begins with these same ocean conditions. The "snapshot" and "transient"-initialized coupled experiments differ only in their ice-dynamic parameter fields, and the "Warm" and "Historical" runs have identical forcing until 2015 and then diverge. Where appropriate we refer to these experiments with designation ***[INITIALIZATION TYPE]_[SLIDING LAW]_[FORCING]***, where ***[INITIALIZATION TYPE]*** is either "SN" for velocity-based (snapshot), or "TR" for thinning-based (transient); ***[SLIDING LAW]*** is either "W" for Weertman or "C" for Coulomb-limited; and ***[FORCING]*** is either "HST" for historical conditions or "WRM" for warm. Where only initializations are considered, we omit the ***[FORCING]*** code.

4. Initialization Results

Mean melt from the 2011–2015 ocean simulation with fixed geometry is shown in Figure 1c. Elevated melt can be seen along an axis extending from the Smith grounding line to the western ice front of Dotson, similar to the channel feature observed in Gourmelen et al. (2017). Melt rates are highest, however, near the grounding line of Kohler and the junction of Dotson and Crosson ice shelves.

Figure 2 compares results for all four initializations (Weertman and Coulomb-limited sliding; snapshot and transient initialization) against velocity and thinning observations. In the snapshot initializations, the velocity misfit norm J_{vel} is reduced by a factor of ∼50 relative to the initial guess, with a favorable visual comparison against observations. However, when forced by surface mass balance from RACMO and mean 2011–2015 melt rates,

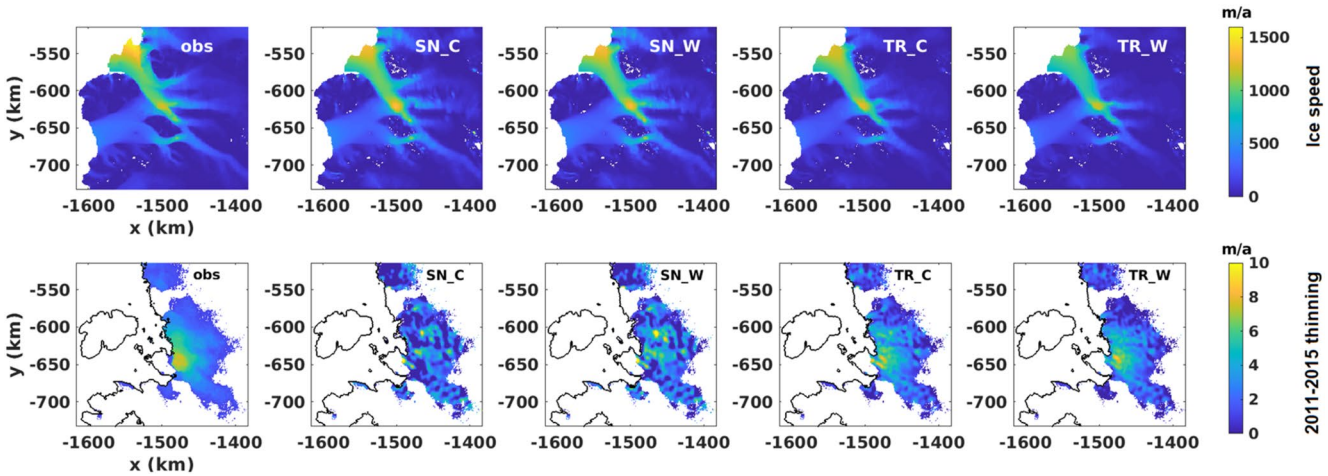

Figure 2. Top row: Observed and modeled velocity of Pope, Smith and Kohler (PSK) glaciers and ice shelves (where the modeled velocity arises from initialization). Bottom row: Observed and modeled 2011–2015 IDI thinning rates for PSK (grounding line shown by black contour). First column shows MEaSUREs velocity magnitude (top) and thinning from Gourmelen et al. (2018) (bottom). Modeled results in subsequent columns correspond to experiment designations from Section 3.3. All modeled thinning rates have a Gaussian filter with a 2 km standard deviation applied.

the resulting grounded thinning rates are a poor match with observations. The transient initializations each see an approximately four-fold reduction in thinning misfit J_{trend}, but also an increase in J_{vel} of a factor of 1.5–2, relative to the parameters from the snapshot initializations. The comparison of J_{vel} between snapshot and transient experiments is uneven, however, as this reflects time-mean velocities in the latter case. Note that the images of 2011–2015 thinning in Figure 2 are not a complete representation of J_{trend}, which also considers misfit over time frames intermediate to the 2011–2015 period.

The cost-function parameters ($\gamma_s^{\beta,B}, \gamma_p^B, \gamma_{tr}$) corresponding to these initializations are in Table 1. For snapshot-based initializations, these parameters were determined through L-"surface" analysis (Goldberg et al., 2019). For the transient initializations it was found that the cost-function lowering was negligible without an increase in $\gamma_s^{\beta,B}$ and a lowering of γ_p^B.

The β and $\bar{B}$ fields corresponding to these initializations are shown in Figure 3; with all results presented as relative to the Coulomb-limited snapshot initialization. For the snapshot initializations, away from the ice shelves and grounding line, $\bar{B}$ largely follows from the temperature model of Van Liefferinge and Pattyn (2013). In terms of the β solutions, for the snapshot solutions, the main difference is a lowering of basal traction near the Smith Glacier grounding line for the Weertman law relative to the Coulomb-limited one. The same is true for the transient solutions. This is an area of low effective stress, hence insensitive to β, and so β is not changed significantly from the initial guess. Meanwhile the transient solutions have large inland variation relative to their snapshot counterparts.

In terms of $\bar{B}$, the difference between snapshot and transient solutions in the Coulomb-limited case is predominantly in the ice shelf, although there are differences in grounded ice close to the grounding line as well. This somewhat explains why γ_p^B, the parameter penalizing variation from the imposed thermal solution, needed lowering for the transient initialization: A viable solution could not be found otherwise. The modification of $\bar{B}$ for the Weertman law is far more extensive: this is due to the fact that a smaller value of γ_p^B was used in the transient Weertman case than in the transient Coulomb-limited case (Table 1). This was because it was seen that a better fit to thinning observations could be achieved—Another run, with the same γ_p^B as for Coulomb-limited, led to an adjustment of $\bar{B}$ closer to that seen for the Coulomb-limited case. It is not clear why an increase in $\gamma_s^{\beta,B}$ was needed but this could be because $\bar{B}$ was less constrained to match with a prior.

Table 1
Cost-Function Parameters Used in Initialization of Ice-Sheet Models in Different Experiments

Param.	Coulomb-limited, snapshot	Weertman, snapshot	Coulomb-limited, transient	Weertman, transient
γ_s^{β}	2.0×10^3	2.0×10^3	1.0×10^5	1.0×10^5
γ_s^{B}	2.0×10^3	2.0×10^3	1.0×10^5	1.0×10^5
γ_p^{B}	2.0×10^2	2.0×10^2	1.0	1.0×10^{-1}
γ^{tr}	N/A	N/A	1.0×10^2	1.0×10^2

Note. The parameters are defined in Section 3.2.

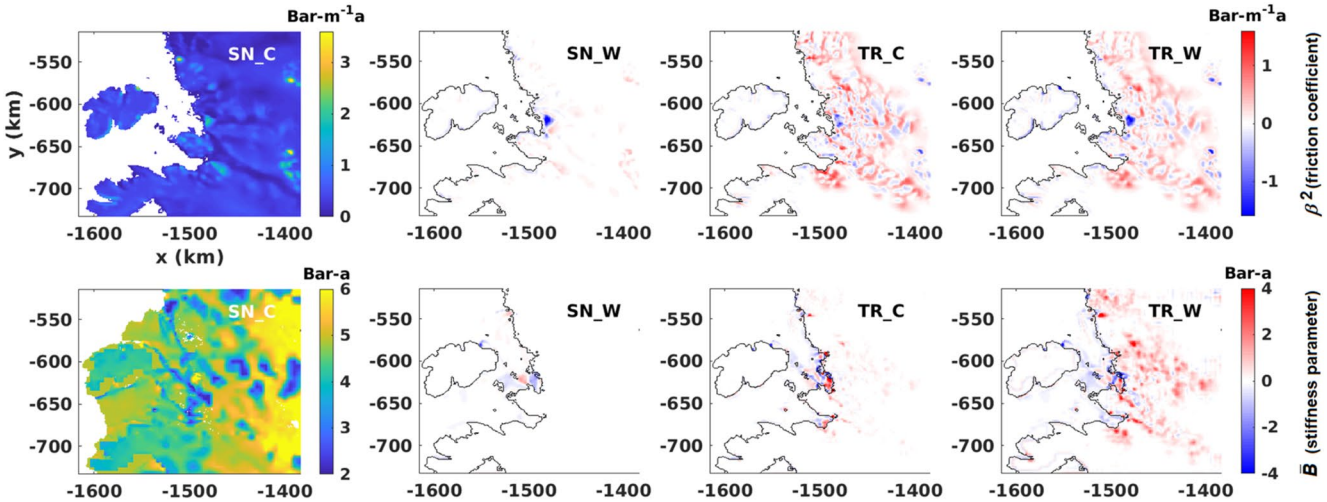

Figure 3. The ice-sheet parameters found through initialization in the four initialization experiments. The top row shows inferred results for β^2, and the bottom for $\bar{B}$. In each panel, the corresponding experiment code is shown (see Section 3.3). Other than the first column, all columns show the difference in the parameter field relative to the Snapshot-initialized, Coulomb-limited (**SN_C**) case.

5. Coupled Modeling: Results

5.1. Short-Term Results

As described in Section 3.3, each sliding-law/initialization pair is initially run to 2015, forced at the ocean boundaries with monthly output from Kimura et al. (2017). As the same boundary conditions are applied to generate the melt used to force the transient initializations, it is expected that the grounded thinning rate in the corresponding coupled runs should be similar to the observed thinning. The top row of Figure 4 compares mean 2011–2015 thinning in coupled simulations to observations. The snapshot-initialized results are similar to those shown in Figure 2, as are results for the Weertman, transient-initialized model (TR_W). However, grounded thinning is far greater for the Coulomb-limited, transient-initialized model (TR_C) than that seen in the actual initializations, with thinning concentrated toward the grounding line.

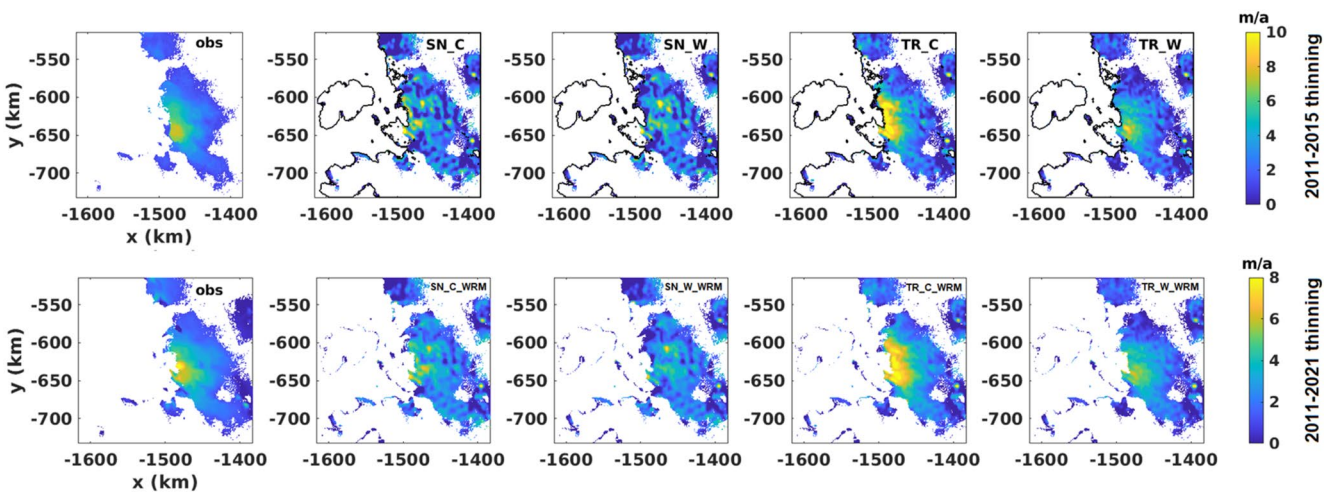

Figure 4. Top row: Observed and coupled-model 2011–2015 IDI thinning rates for Pope, Smith and Kohler (PSK). The first column is annual thinning rate from Gourmelen et al. (2018), and the following columns correspond to the coupled experiments (see Section 3.3). Bottom row: Observed and coupled-model 2011–2021 IDI thinning rates for PSK. The first column is the 2011–2021 CryoSat thinning rate, and following columns correspond to the Warm-forcing coupled experiments. All modeled thinning rates have a Gaussian filter with a 2 km standard deviation applied.

From the perspective of the ice-sheet model, the only difference between the coupled simulation and the initialization run forced by static ice-shelf melt is that the melt (a) evolves in time, and (b) responds to the changing ice-sheet cavity and grounding line. Therefore this mismatch arises from the difference between the sliding laws. The Coulomb-limited sliding law is more sensitive to small changes in thickness near the grounding line, as this modifies effective stress and therefore (in fast-flowing regimes) basal drag, while in the Weertman law, the drag responds only to changes in velocity. Therefore it is possible that either (a) fluctuations in melt affect buttressing more strongly in the Coulomb-limited case, leading to a systematic increase in grounded thinning relative to a time-mean melt, or (b) ice-shelf melt in newly ungrounded areas have a far stronger effect in the Coulomb-limited case. Both Weertman and Coulomb-limited initialization runs exhibited similar levels of grounding line retreat (Supplement Figure S1 in Supporting Information S1), so all coupled runs are exposed to melt under newly-formed ice shelf. This sensitivity to evolving melt can potentially be addressed within our framework by forcing the initial ocean-model run used for initialization with observed changes to ice-shelf draft and grounding line; and by forcing the time-dependent initialization with time-evolving melt. However, such methods are beyond the scope of this study.

The transiently-initialized coupled model incorporates CryoSat thinning rates from 2011 to 2015, but the CryoSat period extends beyond this time interval. Thus, it is worth investigating how well the coupled experiments reproduce elevation change beyond 2015, for a period that was not used to constrain any of the initializations. The bottom row of Figure 4 compares mean 2011–2021 thinning in coupled simulations against CryoSat altimetry (Shepherd et al., 2019) within the Smith IDI region. Holes in the 5-km altimetry product are first filled with bilinear interpolation and the result is interpolated to our grid. Still, the overall best fit is in the transient-initialized Weertman model, with the Coulomb-limited model showing too-high thinning near the grounding line. The snapshot-initialized model mean thinning still has small-scale features, but they are less prominent than over the 2011–2015 period. The results shown are for the Warm-forced runs but the Historically-forced results are nearly identical—Suggesting that melt does not play a strong role in grounded-ice evolution over subdecadal time scales.

5.2. Multidecadal Results

Figure 5a compares annually averaged rates of change of Volume above Floatation (*VAF*; Dupont and Alley (2005)) for snapshot-and transiently-initialized models with Historical and Warm forcing for the Coulomb-limited sliding law. Here, *VAF* is measured only within the IDI region (boundary shown in Figure 6), and does not represent grounded volume for the entire catchment. The 4-year periodicity of the Historic forcing manifests as a "sawtooth" shape in the *VAF* loss rate as well as in basal mass loss (Figure 5b).

Over the first 4 years, the mean *VAF* loss rate for the transiently-coupled runs is 32.9 km^3/a, while for the snapshot-coupled runs it is 21.5 km^3/a. Both disagree with the observed 29.7 km^3/a, but the transiently-coupled rate is significantly closer, despite the anomalously high grounding line-focused thinning. *VAF* loss rate in the Historically-forced, snapshot-initialized run (**SN_C_HST**) increases steadily over the first ∼15 years before dropping slightly and leveling off. By contrast, in the **TR_C_HST** , the *VAF* rate changes little over the first 15 years and then drops rapidly to the point of closely matching the snapshot-initialized run. The Warm-forced experiments are somewhat similar, although with greater loss rates. In both runs, the *VAF* loss rate increases when persistent 2007 forcing is applied, but the adjustment is much greater in **SN_C_WRM** run than in **TR_C_WRM**. After this point, the *VAF* loss rate has similar trajectories in both runs, although loss rates are larger for the transiently-initialized run.

Time series of melt for the two Historically-forced runs are almost indistinguishable (Figure 5b), suggesting that any differences in ice-sheet evolution do not strongly affect ice-shelf geometry (or at least not in a way that affects melt). In both Warm-forced runs, melt increases significantly, almost doubling in annual mean relative to the 2011–2015 average. After this melt rates steadily drop, likely due to ice-shelf thinning leading to less area exposed to warm waters, and lessening of thickness gradients, driving weaker melt water flow. Melt trajectories only begin to diverge after 2050, with transiently-initialized melt rates only slightly larger. In Figure 5c we plot total grounded area (within the IDI region only) for all four experiments. From these trajectories a separation of time scales is apparent. Over the first decade the differences between runs are very much determined by the type of initialization. Once forcings change, the snapshot-initialized runs slowly begin to diverge, as do the transiently-initialized runs. After this, the loss rates of the Historically-forced runs largely mirror each other, as do those of

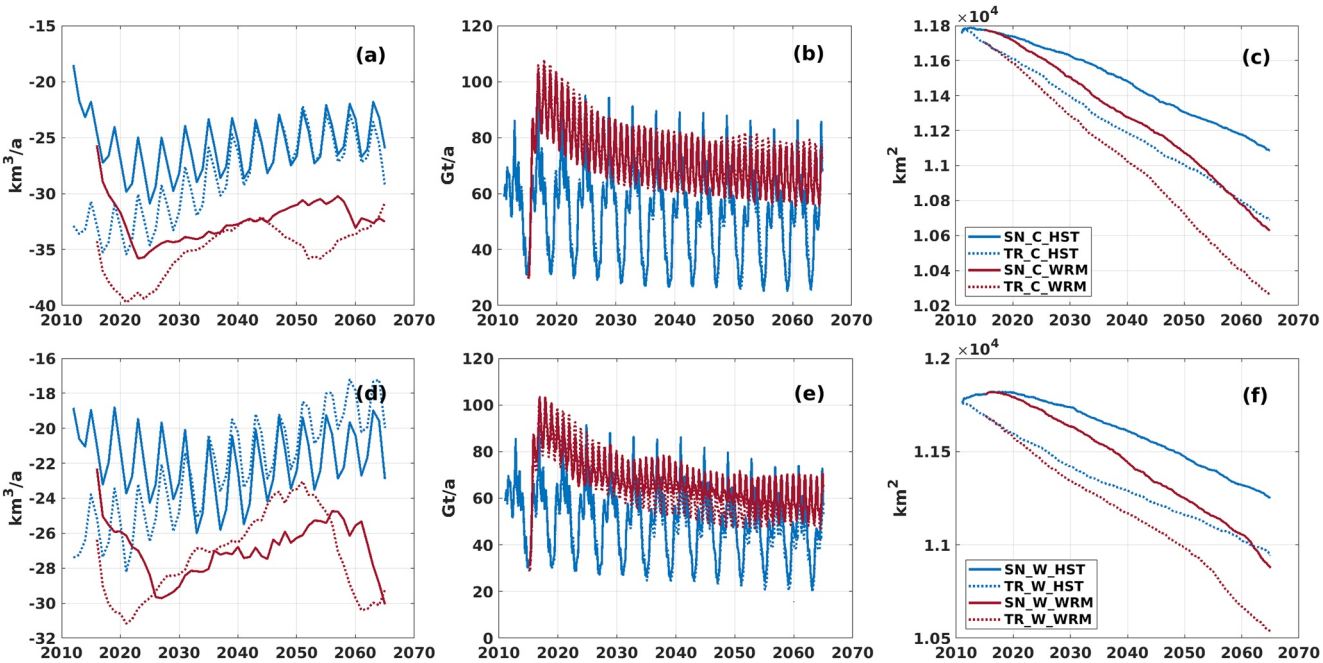

Figure 5. (a) *VAF* rate of change in the coupled simulations with Coulomb-limited sliding (calculation limited to IDI region). (b) Total basal mass loss for these coupled simulations. (c) Grounded area within the IDI region for these coupled simulations. Legend in (c) applies to all panels. (d–f) similar for the coupled simulations with Weertman sliding.

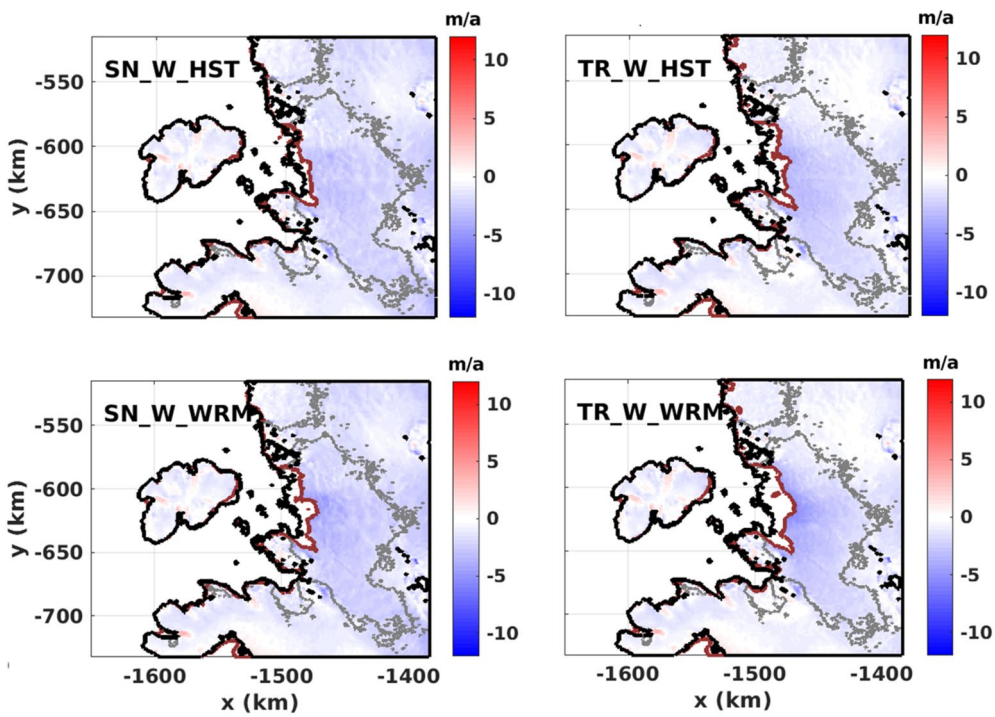

Figure 6. Mean grounded thinning rates (shading) and final grounding line position (red contour) for the Coulomb-limited coupled experiments (experiment designation is given in each panel). In all panels the initial grounding line (solid black contour) and IDI region boundary (gray contour) are shown.

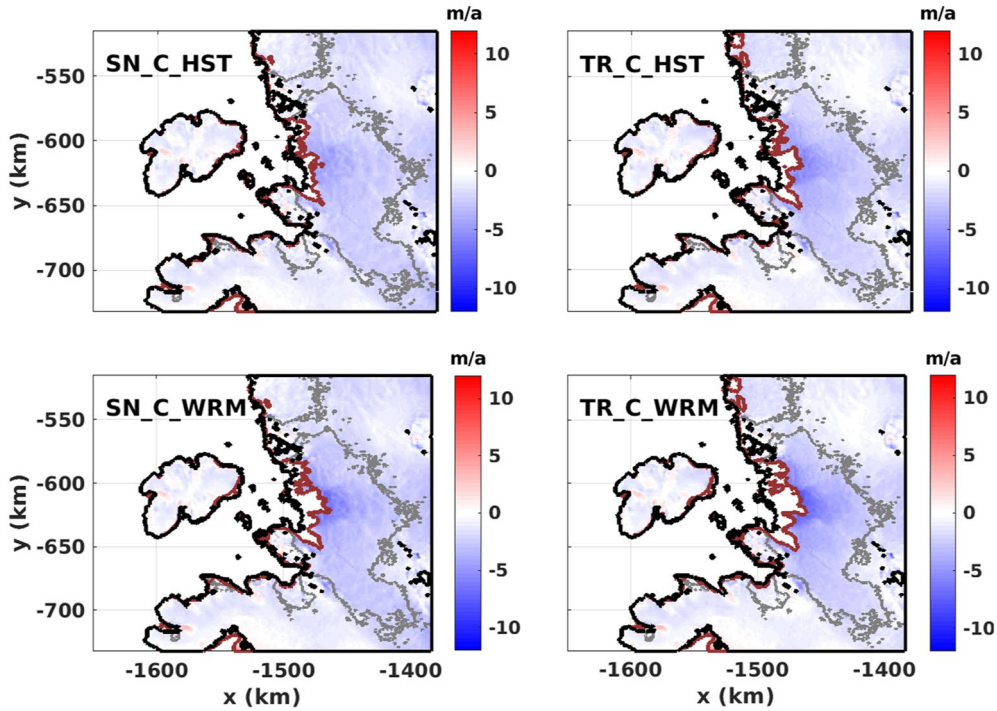

Figure 7. Similar to Figure 6 for coupled simulations with Weertman sliding.

the Warm-forced runs. Owing to the initial decades, however, overall grounding line retreat varies as much with the initialization method as with forcing.

In comparing the final states of the simulations (Figures 6 and 7), the transiently-initialized runs exhibit similar grounding line retreat patterns to the respective snapshot-initialzsed runs with identical forcing. Similarly, the average grounded thinning rate is similar for both Historically-forced runs and also for both Warm-forced runs, respectively. It appears as though between snapshot-initialized and transiently-initialized experiments, the former exhibit similar trajectories to the latter, largely determined by oceanic forcing, but delayed by approximately a decade. In the Historically-forced runs, retreat rates are very similar at the end of the simulation but cumulative grounding line retreat of Smith Glacier is more advanced for **TR_C_HST**. In the Warm-forced runs, **TR_C_WRM** undergoes elevated retreat in ∼2045–2050 (Figure 5a which is related to a local deepening in the bed under Smith Glacier (Figure 8b; see also Figure S2 in Supporting Information S1). **SN_C_WRM** seems to exhibit similar behavior, but it is simply delayed until ∼2060.

Figures 5d–5f and 7 show results comparable to those of Figures 5a–5c and 6, but for the Weertman simulations. Qualitatively, the results are very similar: trends in the *VAF* loss rate are initially determined by the initialization type, but over approximately 10–15 years, the climate forcing becomes more important. Quantitatively there are differences: the 2011–2015 mean *VAF* loss rate is 20 km^3/a for the snapshot-initialized run and 26.4 km^3/a for the transient, with a maximum Warm-forced loss rate of 32 km^3/a (as opposed to 40 km^3/a for the Coulomb-limited law). Over the last decade of simulation, rates of grounded volume loss for **TR_W_HST** drop slightly below those of **SN_W_HST**, although both remain similar and much lower than in the Warm-forced runs. Spatial thinning rates are also smaller than in the Coulomb-limited runs. Grounding-line retreat is comparable to that of the Coulomb-limited runs—Although grounding line morphology is much smoother in the Weertman case.

The degree to which the presence and transport of warm water within the cavity is controlled by bed topography can be seen from inspection of bottom water temperatures at different points in the coupled simulations. This is examined in the context of the Coulomb-limited runs but results for Weertman are similar as the ocean physics are the same and the degree of grounding line retreat is similar. Figure 8a shows bottom temperatures in the Warm-forced, transiently-initialized, Coulomb-limited run 2.5 years after the warm boundary conditions were introduced (i.e., a period sufficient for the warm conditions to penetrate into the cavity, but before the geometry has

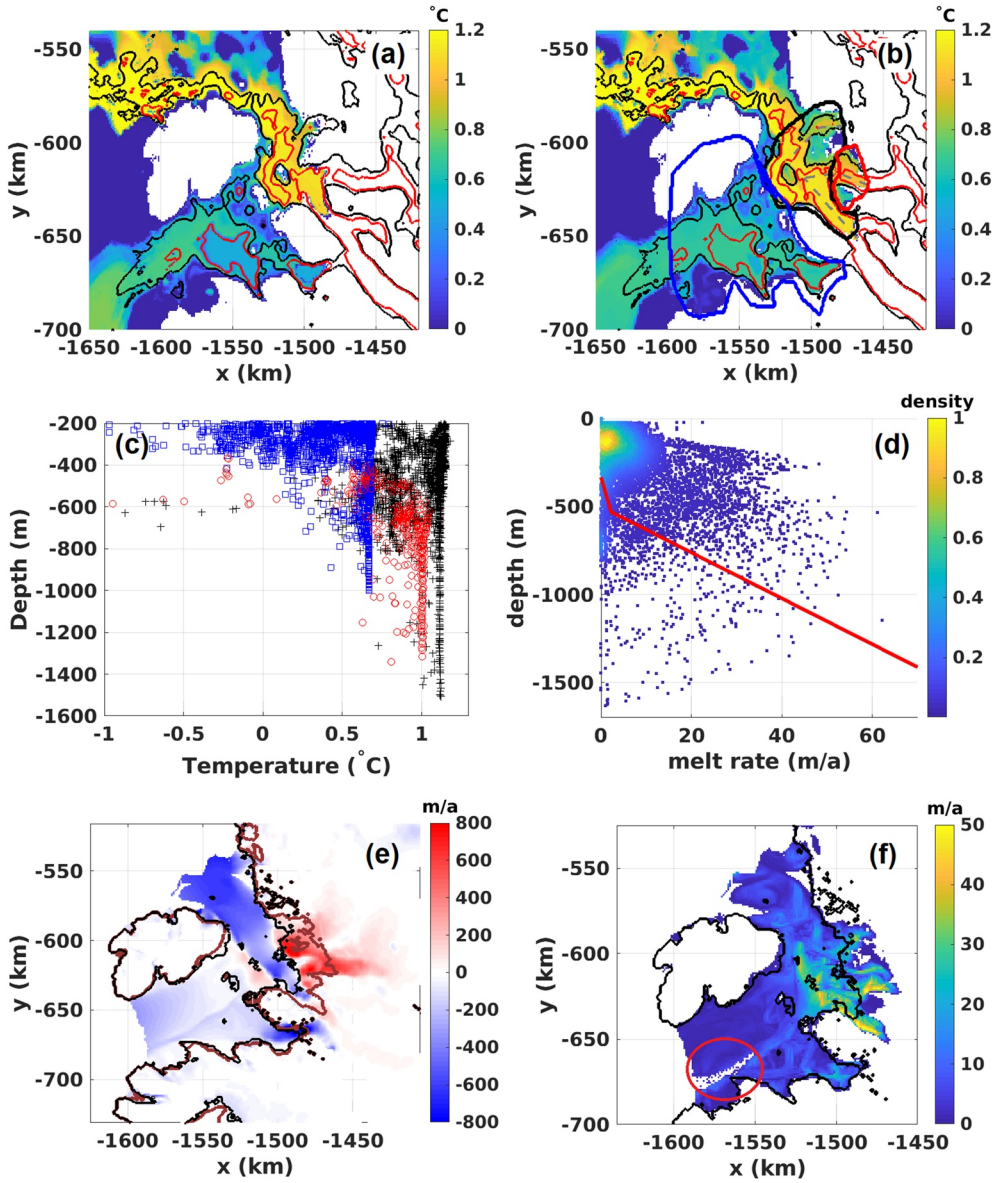

Figure 8. (a) Ocean bottom temperature 2.5 years after 2007 boundary conditions are introduced. (b) Final ocean bottom temperature in experiment **TR_C_WRM**, with 800 m (black) and 1,050 m (red) depth contours. Thick contours indicate (by color) the locations of depth-temperature pairs in (c). Dashed gray lines indicate the locations of the transects in Figure S1 in Supporting Information S1. (c) Scatter plot of depth versus bottom temperature for Dotson ice shelf (blue square), inner Crosson ice shelf (black hatches), and the portion of Smith Glacier behind its deep sill (red circles). (d) Depth-melt rate scatter over the final month of **TR_C_WRM** (point density represented by shading) and melt-depth parameterization from Joughin et al. (2010) (*cf.* (Figure 2e of Lilien et al., 2019)). (e) Total change in ice surface speed during **TR_C_WRM**. (f) Final melt rate in**TR_C_WRM**. Red-circled area indicates melting through of Dotson ice shelf.

changed appreciably from initialization). Warm (>1°C) water is transported from the eastern Amundsen through a deep trough underlying the western margin of Crosson, as suggested by T. A. Jordan et al. (2020), with access to the grounding lines of Pope and Smith glaciers and Kohler East. Kohler West is exposed to the somewhat cooler conditions under Dotson as a result of a sill separating the ice shelves (Figure 8b). As the grounding lines of Pope, Smith and Kohler East retreat, surrounding waters flood the new cavities and determine melt rates under newly exposed ice shelf area, as seen at the end of the 54-year run (Figure 8b; see also Figure S2 in Supporting Information S1). At Pope, melting near the grounding line is relatively low, likely due to a shallow bed which blocks the warmest waters. Melting is greater at the Smith grounding line, although a small sill prevents waters

deeper than ∼1,000 m from reaching the grounding line, resulting in bottom temperatures that are slightly cooled relative to Kohler East (∼1°C vs. 1.2°C). Despite the strong correspondence between depth and bottom temperature (in instances where bottom waters are not topographically blocked; Figure 8c), it can be seen from Figure 8d that there is not a strong correlation between depth and the melt rate.

It is clear that melting and grounding line retreat in the coupled simulation impacts the speed of the glaciers and ice shelves as well as their mass balance. With the exception of Kohler West, all three glaciers increase in speed (Figure 8e). The acceleration of Kohler East is modest compared to that of Pope and Smith, however, despite it is undergoing a similar degree of grounding line retreat. In Dotson ice shelf, a large portion of the channelized-melt region has essentially melted through, as indicated by the absence of melt (Figure 8f, red circled area; see also Section 3.1.3), in line with the predictions of Gourmelen et al. (2017). In the snapshot-initialized Warm-forced run, the channel melts through too as well as in the Historically-forced runs, but to a lesser extent (not shown). The fingerprint of this thickness loss can be seen in the form of a discontinuity in acceleration across the channelized region (Figure 8e), but the impact is relatively minor, suggesting that the melt-through of the channel plays little role in the retreat of the PSK glaciers.

6. Discussion

6.1. Impacts of Initialization, Ice Dynamics and Climate Forcing

In our study we consider different types of coupled model initialization, different forcing scenarios, and different types of ice-bed interaction (in the form of sliding laws). In the coupled experiments the transiently-and snapshot-initialized runs initially differ quite strongly despite (initially) having identical forcing, with the rate of grounded volume (VAF) loss in the transiently-initialized model much closer to observed values. However, as the system evolves, the runs begin to diverge based on the forcing scenario, and after ∼15–20 years, the *VAF* loss rates of the Historically-forced runs begin to align, as do those of the Warm-forced runs. Still, cumulative contribution to the sea level is affected by these initial decades.

The Historically-forced runs tend toward a *VAF* loss rate smaller than that observed over 2011–2015 (∼24–26 km^3/a vs. 29.7 km^3/a). This is despite the fact that they are forced with conditions from the same period. Very likely, 2011–2015 *VAF* loss was a result of a combination of forcing over this interval and that of previous years. Snow et al. (2017) showed that ice sheets respond most strongly to forcing on time scales equivalent to the residence time of the ice shelf, which is on the order of several decades for Amundsen ice shelves.

Goldberg et al. (2015) found that PSK retreat in the early 21st century was largely controlled by the dynamic state of the system, rather than by ice-shelf thinning. Those results are not inconsistent with the findings of the present study. During 1996–2011, the grounding line retreated over a relatively broad ice plain with ice close to floatation. Now that the grounding line is retreating into narrow troughs, retreat is likely more closely coupled to changes in buttressing. However this low sensitivity of multidecadal ice loss to initialization is not necessarily representative of other ice-stream systems. Robel et al. (2019) showed that future loss from Thwaites Glacier is highly sensitive to uncertainty in ocean-driven melt, due to inherent instability; and as such, it may be sensitive to small differences in initialization as well.

The convergence of the snapshot-and transiently-initialized loss rates in the Warm-and Historically-forced runs suggests that initialization via snapshot methods may be sufficient for long-term projections of marine ice sheet loss, even if results are less accurate over the initial decades. Near-term accuracy, however, is important for verifying the predictability of ice-sheet models. In our transient-initialized experiments, the coupled model with Weertman sliding was able to reproduce mean 2011–2021 thinning, using 2011–2015 data as a constraint. Meanwhile thinning in the Coulomb-limited model was overestimated (both over the analysis period and the 2011–2021 period). This may be due to issues with the initialization process rather than the sliding law itself. Still, it is clear that the choice of sliding law has a strong and sustained impact on grounded ice volume loss (Figures 5a and 5d)), and being able to determine the most appropriate sliding law based on observation is of key importance.

6.2. Coupled Modeling and Implications for Parameterized Melt

Our study makes use of a coupled ice-ocean model, as opposed to using an ice-sheet model with a parameterization of ocean-driven melt. Such parameterizations are often depth-dependent in nature for purposes of

simplicity (Dos Santos et al., 2021; Favier et al., 2014; Joughin et al., 2010; Seroussi et al., 2017) but sometimes take account of spatial variation such as far-field hydrography or distance to grounding line (e.g., Lazeroms et al., 2018; Pelle et al., 2019; Reese et al., 2018; Snow et al., 2017). Our modeled melt does not exhibit a strong melt-depth relationship; at the end of the warm-forced transiently-initialized run, the melt-depth correlation has an R^2 of 0.1 (Figure 8e). In contrast, modeling of ice-ocean interactions under Thwaites ice shelf in Seroussi et al. (2017) yielded a melt-depth relationship with an R^2 of 0.87. There are a number of possible reasons for this discrepancy. The lack of relationship could reflect the combination of output from two ice shelves with very different ocean conditions at the shelf fronts, although restricting the analysis to either Dotson or Crosson yields R^2 values of 0.17 and 0.04, respectively. It could alternatively arise from the specific geometries of Crosson and Dotson, or from the fact that in our model, the melt rate depends on under-ice speeds whereas in Seroussi et al. (2017), melt is velocity-independent.

Lilien et al. (2018) forces an ice-sheet model of the PSK glaciers with depth-dependent parameterizations. In particular, forcing with a parameterization based on Joughin et al. (2010) (Figure 8e) yields grounding line retreat of ∼30 km between 2020 and 2070 at Kohler East (their Figure 6; note Kohler East is referred to as "Smith"), which is similar to the retreat seen in our experiments. It is of note that below ∼1,000 m our melt-depth profile is in general lower than that predicted by the Joughin et al. (2010) parameterization whereas above ∼600 m it is predominantly higher. The fact that both yield similar levels of retreat for Kohler East may reflect that the parts of the ice shelf most sensitive to melt are not necessarily the deepest (Goldberg et al., 2019). Meanwhile we see very little (∼5 km) retreat of Kohler West—Referred to as "Kohler" by Lilien et al. (2018)—Whereas their study saw moderate (10 km) retreat until 2080, followed by fast retreat as the grounding line joined with that of Kohler East. This may be due to the spatially uniform melt parameterization used by the authors, which imposes high melt at the Kohler West grounding line. De Rydt & Gudmundsson, 2016 similarly found that simple depth-dependent parameterizations yield high melt near the grounding line, leading to overestimates of retreat.

The coupling in our model is synchronous, in contrast with previous coupled modeling studies of Amundsen Sea glaciers. It is unlikely that an asynchronously coupled model would exhibit significantly different behavior, as the system does not exhibit fast time scales requiring that ocean and ice evolution be coupled on an hourly or daily temporal scale. Still, the sill under Smith Glacier (uncovered due to ice-sheet retreat) and the slightly lower temperatures on the upstream side demonstrate the importance of a coupling scheme that accurately represents the flooding of newly exposed cavity area. A scheme which initializes new parts of the cavity with a predefined profile (Goldberg et al., 2012a) could have a temperature bias in such areas. Extrapolation from nearby cells (De Rydt & Gudmundsson, 2016; Seroussi et al., 2017) may be suitable, as long as the extrapolation respects topographic barriers.

6.3. Mass Loss and Sensitivity of the PSK Region

Our warm-forced experiments, while not a prediction of future conditions, are intended as an extreme scenario for the region under near-term climate change. In the transiently-initialized, Coulomb-limited simulation (**TR_C_WRM**), the region of high observed thinning (*cf.* Figure 2) loses 1,750 km^3 of volume above floatation—Equivalent to ∼5 mm of sea level rise. There is little sign of slowdown of retreat over the 54-year period—Though at the same time, aside from heightened retreat over a small over-deepening, the system does not exhibit signs of strongly accelerating retreat either. This is despite the fact that both Kohler and Smith Glaciers overlie deep bathymetric troughs, and that Dotson ice shelf completely melts through along its margin.

A possible reason for the lack of "runaway retreat" may be that warm bottom waters are not always free to circulate within the cavity, for instance under Smith Glacier where a local bathymetric high at ∼1,000 m depth prevents deeper waters from accessing the grounding line, potentially limiting melt rates. Another, may be the strong level of buttressing which acts on newly floating parts of the ice shelf. Kohler East, which has no barriers to warm water entry, retreats strongly in **TR_C_WRM** (as it does in all experiments), resulting in a large loss of basal resistance (Lilien et al., 2019), and yet the grounded portion upstream of the grounding line experiences relatively little acceleration. The newly-created floating "inlet" is ∼10 km wide, and thus strong buttressing is felt. In addition, the trough under Kohler, while deep, does not significantly deepen inland of the 2011 grounding line. However, with the trough widening upstream, subsequent retreat may lead to acceleration of mass loss. Similarly, if the Kohler West grounding line retreat continues, it could join with Kohler East, further accelerating retreat by widening the "inlet", and also potentially allowing a pathway for warm water into Dotson. Given modeled retreat

rates, it is not inconceivable that this could happen in the next ∼100 years. However, warming at Kohler West sufficient to cause large-scale retreat would likely require strong warming of inflow from Dotson-Getz trough.

It has been shown (Goldberg et al., 2019) that sensitivity of grounded volume to thinning of Dotson is limited, suggesting that melt-through might have little impact on the PSK glaciers. Effects such as calving and ice-shelf breakup are not included in this model, however, so we cannot discount a potentially larger loss of shelf volume in the coming decades.

7. Conclusions

We have applied a synchronously coupled model of ice-ocean interactions to the Pope, Smith and Kohler (PSK) region of the Amundsen sector, West Antarctica. Different sliding laws and approaches to coupled initialization have been used, and two different forcing scenarios have been applied from 2015 onwards. Under the warmer of the two scenarios, the region undergoes significant mass loss over a 50-year period. Kohler and Smith Glaciers in particular undergo extensive grounding line retreat (on the order of 20–30 km), but future retreat may be limited, by buttressing effects on Kohler and by a sill under Smith preventing the deepest and warmest waters from accessing the grounding line. It seems likely that the channelized feature on Dotson ice shelf will melt through, although in our simulations, this melt-through does not drive strong retreat. Still, it is possible that unresolved processes such as catastrophic ice-shelf collapse might lead to extensive mass loss.

Constraining the ice-sheet model with both velocity and thinning rates leads to a dynamic state more consistent with observations in terms of large-scale ice loss. After approximately 1–2 decades, however, the evolution of the system is largely determined by large-scale forcing rather than the initialization method. This has implications both for the stability of the PSK glaciers, as well as the ability of coupled ice-sheet models to accurately predict century-scale behavior. However, given observational limitations, confidence in such simulations will rely on near-term (1–2 decades) predictive skill of coupled simulation. As such, it may be important to incorporate decadal-scale observations into coupled initialization, rather than relying on "snapshot" calibrations. Moreover, it is possible that the PSK glaciers are inherently stable, and this is the reason for insensitivity to initialization; and the mode of initialization may be more critical elsewhere.

Data Availability Statement

The code used for investigations is a modified version of MITgcm, which can be accessed through Zenodo (https://doi.org/10.5281/zenodo.5777460). The OpenAD code is accessible from https://www.mcs.anl.gov/OpenAD. BedMachine data are available at https://nsidc.org/data/nsidc-0756. Output availability information for (Kimura et al., 2017) is given in their publication. CryoSat data are available at ftp://sciencepds. cryosat.esa.int and http://www.cpom.ucl.ac.uk/. Gridded Antarctic Ice Sheet temperature estimates are available from F. Pattyn on request. Modeled output of initialization experiments are included as supplementary material and output of all coupled experiments can be found at https://doi.org/10.5285/4B2910BD-19DB-4A15-A003-88F61137D8EC.

Acknowledgments
D.N.G acknowledges NERC Standard Grant NE/T001607/1 and NSF ITGC Grant PROPHET. P.R.H. acknowledges support from NERC Standard grant NE/S010475/1. We thank the Editor Olga V. Sergienko as well as the Associate Editor for their assistance and management of the review process and for helpful comments on the manuscript, and we thank Ralph Timmermann and two anonymous reviewers for their incredibly insightful reviews.

References

Arthern, R. J., Hindmarsh, R. C. A., & Williams, C. R. (2015). Flow speed within the Antarctic ice sheet and its controls inferred from satellite observations. *Journal of Geophysical Research: Earth Surface*, *120*(7), 1171–1188. https://doi.org/10.1002/2014JF003239

Asay-Davis, X. S., Cornford, S. L., Durand, G., Galton-Fenzi, B. K., Gladstone, R. M., Gudmundsson, G. H., et al. (2016). Experimental design for three interrelated marine ice sheet and ocean model intercomparison projects: MISMIP v. 3 (MISMIP +), ISOMIP v. 2 (ISOMIP +) and MISOMIP v. 1 (MISOMIP1). *Geoscientific Model Development*, *9*(7), 2471–2497. https://doi.org/10.5194/gmd-9-2471-2016

Cornford, S. L., Seroussi, H., Asay-Davis, X. S., Gudmundsson, G. H., Arthern, R., Borstad, C., et al. (2020). Results of the third marine ice sheet model intercomparison Project (MISMIP+). *The Cryosphere*, *14*(7), 2283–2301. https://doi.org/10.5194/tc-14-2283-2020

Dansereau, V., Heimbach, P., & Losch, M. (2014). Simulation of subice shelf melt rates in a general circulation model: Velocity-dependent transfer and the role of friction. *Journal of Geophysical Research: Oceans*, *119*(3), 1765–1790. https://doi.org/10.1002/2013JC008846

Depoorter, M. A., Bamber, J. L., Griggs, J. A., Lenaerts, J. T. M., Ligtenberg, S. R. M., van den Broeke, M. R., & Moholdt, G. (2013). Calving fluxes and basal melt rates of Antarctic ice shelves. *Nature*, *502*(7469), 89–92. https://doi.org/10.1038/nature12567

De Rydt, J., & Gudmundsson, G. H. (2016). Coupled ice shelf-ocean modeling and complex grounding line retreat from a seabed ridge. *Journal of Geophysical Research: Earth Surface*, *121*(5), 865–880. https://doi.org/10.1002/2015JF003791

De Rydt, J., Holland, P. R., Dutrieux, P., & Jenkins, A. (2014). Geometric and oceanographic controls on melting beneath pine island Glacier. *Journal of Geophysical Research: Oceans*, *119*(4), 2420–2438. https://doi.org/10.1002/2013JC009513

Dos Santos, T. D., Barnes, J. M., Goldberg, D. N., Gudmundsson, G. H., & Morlighem, M. (2021). Drivers of change of Thwaites Glacier, West Antarctica, between 1995 and 2015. *Geophysical Research Letters*, *1*(20), 11. https://doi.org/10.1029/2021GL093102

Dupont, T. K., & Alley, R. (2005). Assessment of the importance of ice-shelf buttressing to ice-sheet flow. *Geophysical Research Letters*, *32*(4), L04503. https://doi.org/10.1029/2004GL022024

Dutrieux, P., De Rydt, J., Jenkins, A., Holland, P., Ha, H., Lee, S., et al. (2014). Strong sensitivity of pine island ice-shelf melting to climatic variability. *Science*, *343*(6167), 174–178. https://doi.org/10.1126/science.1244341

Dutrieux, P., Vaughan, D. G., Corr, H. F. J., Jenkins, A., Holland, P. R., Joughin, I., & Fleming, A. H. (2013). Pine Island glacier ice shelf melt distributed at kilometre scales. *The Cryosphere*, *7*(5), 1543–1555. https://doi.org/10.5194/tc-7-1543-2013

Farinotti, D., Huss, M., Fürst, J. J., Landmann, J., Machguth, H., Maussion, F., & Pandit, A. (2019). A consensus estimate for the ice thickness distribution of all glaciers on Earth. *Nature Geoscience*, *12*(3), 168–173. https://doi.org/10.1038/s41561-019-0300-3

Favier, L., Durand, G., Cornford, S. L., Gudmundsson, G. H., Gagliardini, O., Gillet-Chaulet, F., et al. (2014). Retreat of Pine Island Glacier controlled by marine ice-sheet instability. *Nature Climate Change*, *4*(2), 117–121. https://doi.org/10.1038/nclimate2094

Favier, L., Jourdain, N. C., Jenkins, A., Merino, N., Durand, G., Gagliardini, O., et al. (2019). Assessment of sub-shelf melting parameterisations using the ocean–ice-sheet coupled model NEMO (v3.6)–Elmer/Ice (v8.3). *Geoscientific Model Development*, *12*(6), 2255–2283. https://doi.org/10.5194/gmd-12-2255-2019

Fox-Kemper, B., & Menemenlis, D. (2008). Can large eddy simulation techniques improve mesoscale rich ocean models. *Ocean Modeling in an Eddying Regime, Geophysical Monogr*, *177*, 319–337. https://doi.org/10.1029/177GM19

Fretwell, P., Pritchard, H. D., Vaughan, D. G., Bamber, J. L., Barrand, N. E., Bell, R., et al. (2013). Bedmap2: Improved ice bed, surface and thickness datasets for Antarctica. *The Cryosphere*, *7*(1), 375–393. https://doi.org/10.5194/tc-7-375-2013

Fürst, J. J., Durand, G., Gillet-Chaulet, F., Merino, N., Tavard, L., Mouginot, J., et al. (2015). Assimilation of Antarctic velocity observations provides evidence for uncharted pinning points. *The Cryosphere*, *9*(4), 1427–1443. https://doi.org/10.5194/tc-9-1427-2015

Gilbert, J. C., & Lemaréchal, C. (1989). Some numerical experiments with variable-storage quasi-Newton algorithms. *Mathematical Programming*, *45*(3), 407–435. https://doi.org/10.1007/BF01589113

Goldberg, D. N. (2011). A variationally-derived, depth-integrated approximation to a higher-order glaciological flow model. *Journal of Glaciology*, *57*(201), 157–170. https://doi.org/10.3189/002214311795306763

Goldberg, D. N., Gourmelen, N., Kimura, S., Millan, R., & Snow, K. (2019). How accurately should we model ice shelf melt rates? *Geophysical Research Letters*, *46*(1), 189–199. https://doi.org/10.1029/2018GL080383

Goldberg, D. N., & Heimbach, P. (2013). Parameter and state estimation with a time-dependent adjoint marine ice sheet model. *The Cryosphere*, *7*(6), 1659–1678. https://doi.org/10.5194/tc-7-1659-2013

Goldberg, D. N., Heimbach, P., Joughin, I., & Smith, B. (2015). Committed retreat of Smith, Pope, and Kohler Glaciers over the next 30 years inferred by transient model calibration. *The Cryosphere*, *9*(6), 2429–2446. https://doi.org/10.5194/tc-9-2429-2015

Goldberg, D. N., Little, C. M., Sergienko, O. V., Gnanadesikan, A., Hallberg, R., & Oppenheimer, M. (2012a). Investigation of land ice-ocean interaction with a fully coupled ice-ocean model, Part 1: Model description and behavior. *Journal of Geophysical Research-Earth Surface*, *117*(F2), F02037. https://doi.org/10.1029/2011JF002247

Goldberg, D. N., Little, C. M., Sergienko, O. V., Gnanadesikan, A., Hallberg, R., & Oppenheimer, M. (2012b). Investigation of land ice-ocean interaction with a fully coupled ice-ocean model, Part 2: Sensitivity to external forcings. *Journal of Geophysical Research-Earth Surface*, *117*(F2), F02038. https://doi.org/10.1029/2011JF002246

Goldberg, D. N., Narayanan, S. H. K., Hascoet, L., & Utke, J. (2016). An optimized treatment for algorithmic differentiation of an important glaciological fixed-point problem. *Geoscientific Model Development*, *9*(5), 1891–1904. https://doi.org/10.5194/gmd-9-1891-2016

Goldberg, D. N., Snow, K., Holland, P., Jordan, J., Campin, J.-M., Heimbach, P., et al. (2018). Representing grounding line migration in synchronous coupling between a marine ice sheet model and a z-coordinate ocean model. *Ocean Modelling*, *125*, 45–60. https://doi.org/10.1016/j.ocemod.2018.03.005

Gomez, N., Mitrovica, J. X., Huybers, P., & Clark, P. U. (2010). Sea level as a stabilizing factor for marine-ice-sheet grounding lines. *Nature Geoscience*, *3*(12), 850–853. https://doi.org/10.1038/ngeo1012

Gourmelen, N., Escorihuela, M., Shepherd, A., Foresta, L., Muir, A., Garcia-Mondéjar, A., et al. (2018). Cryosat-2 swath interferometric altimetry for mapping ice elevation and elevation change. *Advances in Space Research*, *62*(6), 1226–1242. https://doi.org/10.1016/j.asr.2017.11.014

Gourmelen, N., Goldberg, D. N., Snow, K., Henley, S. F., Bingham, R. G., Kimura, S., et al. (2017). Channelized melting drives thinning under a rapidly melting Antarctic ice shelf. *Geophysical Research Letters*, *44*(19), 9796–9804. https://doi.org/10.1002/2017GL074929

Grosfeld, K., & Sandhager, H. (2004). The evolution of a coupled ice shelf-ocean system under different climate states. *Global and Planetary Change*, *42*(1–4), 107–132. https://doi.org/10.1016/j.gloplacha.2003.11.004

Haseloff, M., & Sergienko, O. V. (2018). The effect of buttressing on grounding line dynamics. *Journal of Glaciology*, *64*(245), 417–431. https://doi.org/10.1017/jog.2018.30

Holland, D. M., & Jenkins, A. (1999). Modelling thermodynamic ice-ocean interactions at the base of an ice shelf. *Journal of Physical Oceanography*, *29*(8), 1787–1800. https://doi.org/10.1175/1520-0485(1999)029

Holland, P. R., Bracegirdle, T. J., Dutrieux, P., Jenkins, A., & Steig, E. J. (2019). West Antarctic ice loss influenced by internal climate variability and anthropogenic forcing. *Nature Geoscience*, *12*(9), 718–724. https://doi.org/10.1038/s41561-019-0420-9

Jacobs, S. S., Jenkins, A., Giulivi, C., & Dutrieux, P. (2011). Stronger ocean circulation and increased melting under Pine Island Glacier ice shelf. *Nature Geoscience*, *4*(8), 519–523. https://doi.org/10.1038/NGEO1188

Jenkins, A., Dutrieux, P., Jacobs, S., Steig, E. J., Gudmundsson, H., Smith, J., & Heywood, K. (2016). Decadal ocean forcing and Antarctic ice sheet response: Lessons from the Amundsen Sea. *Oceanography*, *29*(4), 106–117. https://doi.org/10.5670/oceanog.2016.103

Jenkins, A., Shoosmith, D., Dutrieux, P., Jacobs, S., Kim, T. W., Le, S. H., et al. (2018). West Antarctic Ice Sheet retreat in the Amundsen Sea driven by decadal oceanic variability. *Nature Geoscience*, *11*(10), 733–738. https://doi.org/10.1038/s41561-018-0207-4DO

Jordan, J. R., Holland, P. R., Goldberg, D., Snow, K., Arthern, R., Campin, J. M., et al. (2017). Ocean-forced ice-shelf thinning in a synchronously coupled ice-ocean model. *Journal of Geophysical Research: Oceans*, *123*(2), 864–882. https://doi.org/10.1002/2017JC013251

Jordan, T. A., Porter, D., Tinto, K., Millan, R., Muto, A., Hogan, K., et al. (2020). New gravity-derived bathymetry for the Thwaites, Crosson, and Dotson ice shelves revealing two ice shelf populations. *The Cryosphere*, *14*(9), 2869–2882. https://doi.org/10.5194/tc-14-2869-2020

Joughin, I., Smith, B., & Holland, D. M. (2010). Sensitivity of 21st century sea level to ocean-induced thinning of Pine Island Glacier, Antarctica. *Geophysical Research Letters*, *37*(20), L20502. https://doi.org/10.1029/2010GL044819

Joughin, I., Smith, B. E., & Medley, B. (2014). Marine ice sheet collapse potentially under way for the Thwaites Glacier Basin, West Antarctica. *Science*, *344*(6185), 735–738. https://doi.org/10.1126/science.1249055

Khazendar, A., Rignot, E., Schroeder, D., Seroussi, H., Schodlok, M., Scheuchl, B., et al. (2016). Rapid submarine ice melting in the grounding zones of ice shelves in West Antarctica. *Nature Communications*, *7*(1), 13243. https://doi.org/10.1038/ncomms13243

Kimura, S., Adrian, J., Heather, R., Jenkins, A., Regan, H., Holland, P. R., et al. (2017). Oceanographic controls on the variability of ice-shelf basal melting and circulation of Glacial meltwater in the Amundsen Sea Embayment, Antarctica. *Journal of Geophysical Research: Oceans*, *122*(12), 10131–10155. https://doi.org/10.1002/2017JC012926

Lazeroms, W. M., Jenkins, A., Gudmundsson, G. H., & Van De Wal, R. S. (2018). Modelling present-day basal melt rates for Antarctic ice shelves using a parametrization of buoyant meltwater plumes. *The Cryosphere*, *12*(1), 49–70. https://doi.org/10.5194/tc-12-49-2018

Lenaerts, J. T., Van den Broeke, M., Van de Berg, W., Van Meijgaard, E., & Kuipers Munneke, P. (2012). A new, high-resolution surface mass balance map of Antarctica (1979–2010) based on regional atmospheric climate modeling. *Geophysical Research Letters*, *39*(4), L04501. https://doi.org/10.1029/2011GL050713

Lilien, D. A., Joughin, I., Smith, B., & Gourmelen, N. (2019). Melt at grounding line controls observed and future retreat of Smith, Pope, and Kohler glaciers. *The Cryosphere*, *13*(11), 2817–2834. https://doi.org/10.5194/tc-13-2817-2019

Lilien, D. A., Joughin, I., Smith, B., & Shean, D. E. (2018). Changes in flow of Crosson and Dotson ice shelves, West Antarctica, in response to elevated melt. *The Cryosphere*, *12*(4), 1415–1431. https://doi.org/10.5194/tc-12-1415-2018

Lipscomb, W. H., Price, S. F., Hoffman, M. J., Leguy, G. R., Bennett, A. R., Bradley, S. L., et al. (2019). Description and evaluation of the community ice sheet model (CISM) v2.1. *Geoscientific Model Development*, *12*(1), 387–424. https://doi.org/10.5194/gmd-12-387-2019

Losch, M. (2008). Modeling ice shelf cavities in a z coordinate ocean general circulation model. *Journal of Geophysical Research*, *113*(C8), C08043. https://doi.org/10.1029/2007JC004368

Marshall, J., Hill, C., Perelman, L., & Adcroft, A. (1997). Hydrostatic, quasi-hydrostatic, and nonhydrostatic ocean modeling. *Journal of Geophysical Research*, *102*(C3), 5733–5752. https://doi.org/10.1029/96JC02776

McMillan, M., Shepherd, A., Sundal, A., Briggs, K., Muir, A., Ridout, A., et al. (2014). Increased ice losses from Antarctica detected by CryoSat-2. *Geophysical Research Letters*, *41*(11), 3899–3905. https://doi.org/10.1002/2014GL060111

Milillo, P., Rignot, E., Rizzoli, P., Scheuchl, B., Mouginot, J., Bueso-Bello, J., & Prats-Iraola, P. (2019). Heterogeneous retreat and ice melt of Thwaites Glacier, West Antarctica. *Science Advances*, *5*(1), eaau3433. https://doi.org/10.1126/sciadv.aau3433

Millan, R., Rignot, E., Bernier, V., Morlighem, M., & Dutrieux, P. (2017). Bathymetry of the Amundsen Sea Embayment sector of West Antarctica from operation IceBridge gravity and other data. *Geophysical Research Letters*, *44*(3), 1360–1368. https://doi.org/10.1002/2016GL072071

Morlighem, M., Rignot, E., Binder, T., Blankenship, D., Drews, R., Eagles, G., et al. (2020). Deep glacial troughs and stabilizing ridges unveiled beneath the margins of the Antarctic ice sheet. *Nature Geoscience*, *13*(2), 132–137. https://doi.org/10.1038/s41561-019-0510-8

Mouginot, J., Rignot, E., & Scheuchl, B. (2014). Sustained increase in ice discharge from the Amundsen Sea Embayment, West Antarctica, from 1973 to 2013. *Geophysical Research Letters*, *41*(5), 1576–1584. https://doi.org/10.1002/2013GL059069

Naughten, K. A., De Rydt, J., Rosier, S. H., Jenkins, A., Holland, P. R., & Ridley, J. K. (2021). Two-timescale response of a large Antarctic ice shelf to climate change. *Nature Communications*, *12*(1), 1–10. https://doi.org/10.1038/s41467-021-22259-0

Pegler, S. S. (2018). Suppression of marine ice sheet instability. *Journal of Fluid Mechanics*, *857*, 648–680. https://doi.org/10.1017/jfm.2018.742

Pelle, T., Morlighem, M., & Bondzio, J. H. (2019). Brief communication: PICOP, a new ocean melt parameterization under ice shelves combining PICO and a plume model. *The Cryosphere*, *13*(3), 1043–1049. https://doi.org/10.5194/tc-13-1043-2019

Pelle, T., Morlighem, M., Nakayama, Y., & Seroussi, H. (2021). Widespread grounding line retreat of Totten Glacier, East Antarctica, over the 21st century. *Geophysical Research Letters*, *48*(17), e2021GL093213. https://doi.org/10.1029/2021GL093213

Perego, M., Price, S., & Stadler, G. (2014). Optimal initial conditions for coupling ice sheet models to Earth system models. *Journal of Geophysical Research: Earth Surface*, *119*(9), 1894–1917. https://doi.org/10.1002/2014JF003181

Petty, A. A., Feltham, D. L., & Holland, P. R. (2013). Impact of atmospheric forcing on Antarctic continental shelf Water masses. *Journal of Physical Oceanography*, *43*(5), 920–940. https://doi.org/10.1175/JPO-D-12-0172.1

Reese, R., Gudmundsson, G. H., Levermann, A., & Winkelmann, R. (2018). The far reach of ice-shelf thinning in Antarctica. *Nature Climate Change*, *8*(1), 53–57. https://doi.org/10.1038/s41558-017-0020-x

Rignot, E., Mouginot, J., Morlighem, M., Seroussi, H., & Scheuchl, B. (2014). Widespread, rapid grounding line retreat of pine island, Thwaites, Smith and Kohler glaciers, West Antarctica from 1992 to 2011. *Geophysical Research Letters*, *41*(10), 3502–3509. https://doi.org/10.1002/2014GL060140

Rignot, E., Mouginot, J., & Scheuchl, B. (2011). Ice flow of the Antarctic ice sheet. *Science*, *333*(6048), 1427–1430. https://doi.org/10.1126/science.1208336

Robel, A. A., Seroussi, H., & Roe, G. H. (2019). Marine ice sheet instability amplifies and skews uncertainty in projections of future sea-level rise. *Proceedings of the National Academy of Sciences*, *116*(30), 14887–14892. https://doi.org/10.1073/pnas.1904822116

Scheuchl, B., Mouginot, J., Rignot, E., Morlighem, M., & Khazendar, A. (2016). Grounding line retreat of Pope, Smith, and Kohler Glaciers, West Antarctica, measured with Sentinel-1a radar interferometry data. *Geophysical Research Letters*, *43*(16), 8572–8579. https://doi.org/10.1002/2016GL069287

Schoof, C. (2007). Marine ice sheet dynamics. Part I. The case of rapid sliding. *Journal of Fluid Mechanics*, *573*, 27–55. https://doi.org/10.1017/S0022112006003570

Schoof, C., Davis, A. D., & Popa, T. V. (2017). Boundary layer models for calving marine outlet glaciers. *The Cryosphere*, *11*(5), 2283–2303. https://doi.org/10.5194/tc-11-2283-2017

Sergienko, O. V. (2022). No general stability conditions for marine ice-sheet grounding lines in the presence of feedbacks. *Nature Communications*, *13*(1), 1–6. https://doi.org/10.1038/s41467-022-29892-3

Sergienko, O. V., & Wingham, D. J. (2022). Bed topography and marine ice-sheet stability. *Journal of Glaciology*, *68*(267), 124–138. https://doi.org/10.1017/jog.2021.79

Seroussi, H., Nakayama, Y., Larour, E., Menemenlis, D., Morlighem, M., Rignot, E., & Khazendar, A. (2017). Continued retreat of thwaites glacier, west Antarctica, controlled by bed topography and ocean circulation. *Geophysical Research Letters*, *44*(12), 6191–6199. https://doi.org/10.1002/2017GL072910

Seroussi, H., Nowicki, S., Simon, E., Abe-Ouchi, A., Albrecht, T., Brondex, J., et al. (2019). MIP-Antarctica: An ice sheet model initialization experiment of ISMIP6. *The Cryosphere*, *13*(5), 1441–1471. https://doi.org/10.5194/tc-13-1441-2019

Shepherd, A., Gilbert, L., Muir, A. S., Konrad, H., McMillan, M., Slater, T., et al. (2019). Trends in Antarctic ice sheet elevation and mass. *Geophysical Research Letters*, *46*(14), 8174–8183. https://doi.org/10.1029/2019GL082182

Shepherd, A., Ivins, E., Rignot, E., Smith, B., Van Den Broeke, M., & Velicogna, I. (2018). Mass balance of the Antarctic Ice Sheet from 1992 to 2017. *Nature*, *558*(7709), 219–222. https://doi.org/10.1038/s41586-018-0179-y

Shepherd, A., Wingham, D. J., & Rignot, E. (2004). Warm ocean is eroding West Antarctic ice sheet. *Geophysical Research Letters*, *31*(23), L23402. https://doi.org/10.1029/2004GL021106

Smith, B., Fricker, H. A., Gardner, A. S., Medley, B., Nilsson, J., Paolo, F. S., et al. (2020). Pervasive ice sheet mass loss reflects competing ocean and atmosphere processes. *Science*, *368*(6496), 1239–1242. https://doi.org/10.1126/science.aaz5845

Smith, R. S., Mathiot, P., Siahaan, A., Lee, V., Cornford, S. L., Gregory, J. M., et al. (2021). Coupling the UK Earth System Model to dynamic models of the Greenland and Antarctic ice sheets. *Journal of Advances in Modeling Earth Systems*, *13*(10), e2021MS002520. https://doi.org/10.1029/2021MS002520

Snow, K., Goldberg, D., Holland, P. R., Jordan, J. R., Arthern, R. J., & Jenkins, A. (2017). The response of ice sheets to climate variability. *Geophysical Research Letters*, *44*(23), 11878–11885. https://doi.org/10.1002/2017GL075745

Steig, E. J., Ding, Q., Battisti, D., & Jenkins, A. (2012). Tropical forcing of circumpolar deep water inflow and outlet glacier thinning in the Amundsen Sea Embayment, West Antarctica. *Annals of Glaciology*, *53*(60), 19–28. https://doi.org/10.3189/2012AoG60A110

Timmermann, R., & Goeller, S. (2017). Response to Filchner–Ronne Ice Shelf cavity warming in a coupled ocean–ice sheet model–Part 1: The ocean perspective. *Ocean Science*, *13*(5), 765–776. https://doi.org/10.5194/os-13-765-2017

Van Liefferinge, B., & Pattyn, F. (2013). Using ice-flow models to evaluate potential sites of million year-old ice in Antarctica. *Climate of the Past Discussions*, *9*(3), 2335–2345. https://doi.org/10.5194/cp-9-2335-2013